Swelling-induced bending and pumping in homogeneous thin sheets

Michele Curatolo, and Paola Nardinocchi

Swelling-induced bending and pumping in homogeneous thin sheets

Michele Curatolo[1,a)] and Paola Nardinocchi[2,b)]
[1]*Università di Roma Tre, Roma, Italy*
[2]*Sapienza, Università di Roma, Roma, Italy*

We realize steady curved shapes from homogeneous hydrogel flat structures which are in contact with two environments at different chemical conditions. We numerically investigate the behaviour of beam-like and plate-like structures during the transient state, which realize osmotic pumps. Through numerical experiments, we determine the relationship between the difference in the chemical potentials at the top and bottom of a beam and the curvature of the bent beam as well as the Gaussian curvature of a spherical cap morphed from a flat plate. We also propose an approximate modeling of both the beam and the plate, to evaluate explicitly that relationship and show the good agreement between those formulas and the outcomes of the numerical simulations. *Published by AIP Publishing.* https://doi.org/10.1063/1.5043580

I. INTRODUCTION

Hydrogels swell and contract in response to a wide range of environmental stimuli and, due to their properties, have been intensively studied as one of the most promising materials for multifunctional devices. On the one hand, there is a great choice both in the type of stimuli to employ and in the arrangements of materials and geometric properties.[1] On the other hand, the ability of hydrogels to elastically undergo large deformations and bifurcations widens the spectrum of attainable configurations and effects.

The bending strategy is one of the programming strategies that can be used for planning the morphing based on out-of-plane bending of hydrogel-based slender structures. In thin hydrogel structures arranged in the form of composites which combine constituents with physical or chemical properties different one from each other, shape changes are triggered by the differential swelling of the constituents, combined with an interplay between geometry and mechanics, which may also involve stability issues. As for the bimetal thermostats studied by Timoshenko, the curvature of a hydrogel-based bilayer strip can be programmed; in the latter case, through the control of the swelling ratios, which originate from different polymer compositions.[2–4] Moreover, also complex shape transformations can be programmed by including additional control parameters into the programming strategy, such as oriented fiber fields which make the material response of the hydrogels anisotropic.[5]

An alternative strategy to realize bending in hydrogel structures is based on a non-homogenous exposure of a homogeneous structure to an activation stimulus, as experienced in Refs. 6 and 7. This strategy allows realizing a transient gradient in swelling as the diffusion of the solvent inside the material takes time. As the diffusion is completed, a uniform swelling is attained through the material thickness, and bending is inhibited.

We implemented a different strategy, considering a homogeneous hydrogel structure which is in contact at its top and bottom faces with two environments at different chemical conditions and is not permeable at its edges. Water diffuses into the hydrogel according to the opposite of the gradient of the chemical potential, so realizing an osmotic pump. Assuming that the chemical conditions of the two environments remain unchanged, diffusion never stops; at the steady state, a uniform water flux is attained through the material thickness, and a bent shape with uniform curvature is obtained. Homogeneous hydrogel beam-like structures realize curved shapes, whereas plate-like structures morph into spherical caps.

We numerically investigate the behaviour of the beam-like and plate-like pumps during the transient state by means of a finite element implementation of the mathematical model. Through a series of numerical experiments, we determine the relationship between the difference in the chemical potentials at the top and bottom of the structure and the curvature of the bent beam as well as the Gaussian curvature of the spherical cap. We also propose an extension of the beam-like model presented by one of the authors in Ref. 2, to evaluate explicitly that relationship and show the good agreement between those formulas and the outcomes of the numerical simulations. Finally, inspired by the geometrical issues presented in Ref. 8, and following the idea proposed in Ref. 9, we also evaluate the elastic energy corresponding to the spherical configuration attained by the plate and evaluate explicitly the Gaussian curvature of the spherical cap as the minimum of that energy. The comparison with the numerical outcomes shows that, when the difference in the chemical potentials at the top and bottom of the structure is not too high, the explicit and the numerical solutions are in good agreement.

II. THEORETICAL BACKGROUND

Swelling and de-swelling dynamics is studied starting from the multiphysics model presented and discussed in Ref. 10 and successively refined in Refs. 11–13. The water-polymer

a)michele.curatolo@uniroma3.it
b)paola.nardinocchi@uniroma1.it

mixture is modeled as a homogenized continuum body, allowing for a mass flux of the solvent, as also proposed in Refs. 14–17.

The *dry-reference state* $\mathcal{B}_d$ of the gel is chosen as one of the reference configurations of the continuum body, identified with the region of the Euclidean space $\mathcal{E}$; $X_d \in \mathcal{B}_d \subset \mathcal{E}$ is a material point and $t \in \mathcal{T}$ is an instant of the time interval $\mathcal{T}$. We introduce two state variables: the displacement field $\mathbf{u}_d(X_d,t)$ from $\mathcal{B}_d$ ($[\mathbf{u}_d] = $ m),[18] which gives the actual position $\mathcal{E} \ni x = X_d + \mathbf{u}_d(X_d,t)$ of the point X_d at time t, and the molar water-concentration per unit dry volume $c_d(X_d,t)$ ($[c_d] = $ mol/m^3). The two state variables are coupled through the following volumetric constraint:

$$J_d = \det \mathbf{F}_d = \hat{J}_d(c_d) = 1 + \Omega c_d, \quad (2.1)$$

implying that any change in volume of the gel is accompanied by an equivalent uptake or release of water content. Therein, $\mathbf{F}_d = \mathbf{I} + \nabla \mathbf{u}_d$ is the deformation gradient and Ω is the molar volume of the water ($[\Omega] = $ m^3/mol).

We assume that the free energy ψ per unit dry-volume depends on $\mathbf{F}_d$ through an elastic component ψ_e, and on c_d through a polymer-water mixing energy ψ_m: $\psi = \psi_e + \psi_m$, as prescribed by the Flory–Rehner thermodynamic model.[19,20] Moreover, we introduce a relaxed free-energy ψ_r, which includes the volumetric constraint, as

$$\psi_r(\mathbf{F}_d, c_d, p) = \psi_e(\mathbf{F}_d) + \psi_m(c_d) - p(J_d - \hat{J}_d(c_d)), \quad (2.2)$$

with the pressure p as the reaction to the volumetric constraint, which maintains the volume change J_d due to the displacement equal to the one due to solvent absorption or release $\hat{J}_d(c_d)$.

The constitutive equation for the dry-reference stress $\mathbf{S}_d$ ($[\mathbf{S}_d] = $ Pa $=$ J/m^3) (the stress at the dry configuration $\mathcal{B}_d$) and for the chemical potential μ ($[\mu] = $ J/mol) are derived from (2.2), which yields

$$\mathbf{S}_d = \hat{\mathbf{S}}_d(\mathbf{F}_d) - p\,\mathbf{F}_d^\star = \frac{\partial \psi_e}{\partial \mathbf{F}_d} - p\,\mathbf{F}_d^\star, \quad (2.3)$$

$$\mu = \hat{\mu}(c_d) + p\,\Omega = \frac{\partial \psi_m}{\partial c_d} + p\,\Omega, \quad (2.4)$$

$\mathbf{F}_d^\star = J_d\,\mathbf{F}_d^{-T}$ being the adjoint of the deformation gradient $\mathbf{F}_d$. We assume that the elastic component ψ_e of the free energy has a neo-Hookean form, and the polymer-water mixing energy ψ_m has the Flory–Huggins form

$$\psi_e(\mathbf{F}_d) = \frac{G_d}{2}(\mathbf{F}_d \cdot \mathbf{F}_d - 3), \quad \psi_m(c_d) = \frac{\mathcal{R}T}{\Omega}\,h(c_d), \quad (2.5)$$

with

$$h(c_d) = \Omega\,c_d \log \frac{\Omega\,c_d}{1 + \Omega\,c_d} + \chi\,\frac{\Omega\,c_d}{1 + \Omega\,c_d}, \quad [h] = 1, \quad (2.6)$$

G ($[G] = $ J/m^3) being the shear modulus of the dry polymer, $\mathcal{R}$ ($[\mathcal{R}] = $ J/(K mol)) the universal gas constant, T ($[T] = $ K) the temperature, and χ the Flory parameter. Using (2.4)–(2.6), we can obtain the constitutive equations specific to our energy choice (2.5)

$$\hat{\mathbf{S}}_d(\mathbf{F}_d) = G_d\,\mathbf{F}_d,$$

$$\hat{\mu}(c_d) = \hat{\mu}(J_d) = \mathcal{R}T\left(\log \frac{J_d - 1}{J_d} + \frac{1}{J_d} + \frac{\chi}{J_d^2}\right), \quad (2.7)$$

where, with a light abuse of notation, we wrote the relation for the chemical potential $\mu = \hat{\mu}(c_d)$ in terms of J_d as $\hat{\mu}(J_d)$ by exploiting the volumetric constraint (2.1) between the determinant J_d of the deformation gradient and the water concentration per unit dry volume.

It is worth noting that, with these choices, the dissipation principle is reduced to the following inequality:

$$\mathbf{h}_d(\mathbf{F}_d, c_d, p) \cdot \nabla \mu(c_d, p) \leq 0, \quad \mu(c_d, p) = \hat{\mu}(c_d) + p\,\Omega, \quad (2.8)$$

$\mathbf{h}_d$ ($[\mathbf{h}_d] = $ mol/(m^2 s)) being the reference solvent flux. We assume that it has the following representation form:

$$\mathbf{h}_d = \mathbf{h}_d(\mathbf{F}_d, c_d, p) = -\mathbf{M}(\mathbf{F}_d, c_d)\nabla(\hat{\mu}(c_d) + p\,\Omega), \quad (2.9)$$

with the mobility tensor $\mathbf{M}(\mathbf{F}_d, c_d)$ as a positive definite tensor ($[[\mathbf{M}]] = $ mol^2/(s m J)). In particular, we also assume that $\mathbf{M}$ is isotropic and linearly dependent on c_d, and diffusion always remains isotropic during any process.[10,14,16,17] These assumptions determine the representation of the mobility tensor in terms of the inverse of the Cauchy–Green strain tensor $\mathbf{C}_d$ as

$$\mathbf{M}(\mathbf{F}_d, c_d) = \frac{D}{\mathcal{R}T}\,c_d\mathbf{C}_d^{-1}, \quad \mathbf{C}_d = \mathbf{F}_d^T\mathbf{F}_d, \quad (2.10)$$

with D ($[D] = $ m^2/s) the diffusivity.

Finally, the balance equations of the model are

$$\mathbf{0} = \operatorname{div} \mathbf{S}_d \quad \text{and} \quad \dot{c}_d = -\operatorname{div} \mathbf{h}_d, \quad (2.11)$$

on $\mathcal{B}_d \times \mathcal{T}$. They are supplemented by the boundary conditions on $\partial_t \mathcal{B}_d \times \mathcal{T}$ and $\partial_u \mathcal{B}_d \times \mathcal{T}$,

$$\mathbf{S}_d\,\mathbf{m} = \mathbf{t} \quad \text{and} \quad \mathbf{u}_d = \bar{\mathbf{u}}_d, \quad (2.12)$$

respectively; and on $\partial_q \mathcal{B}_d \times \mathcal{T}$ and $\partial_c \mathcal{B}_d \times \mathcal{T}$,

$$-\mathbf{h}_d \cdot \mathbf{m} = q_s \quad \text{and} \quad \hat{\mu}(c_s) + p\,\Omega = \mu_e, \quad (2.13)$$

respectively, with c_s the concentration field on $\partial_c \mathcal{B}_d$ which is assigned implicitly by controlling the external chemical potential μ_e. The initial conditions,

$$\mathbf{u}_d = \mathbf{u}_{do} \quad \text{and} \quad c_d = c_{do}, \quad (2.14)$$

on $\mathcal{B}_d \times \{0\}$ make the problem doable: $\mathbf{u}_{do}$ and c_{do} are the initial values of the fields $\mathbf{u}_d$ and c_d, respectively. Everywhere, a dot denotes the time derivative and div the divergence operator. Equations (2.11) describe the balance of forces and the balance of water concentration; they are coupled through the volumetric constraint (2.1) and the constitutive equations (2.3)–(2.6). Equations (2.12) are the mechanical boundary conditions on the traction $\mathbf{t}$ and/or displacement $\bar{\mathbf{u}}_d$, with $\mathbf{m}$ denoting the outward unit normal. Equations (2.13) are the chemical boundary conditions on boundary solvent source $q_s = -\mathbf{h}_d \cdot \mathbf{m}$ ($[q_s] = $ mol/(m^{2}s)^2 (Ref. 21) and/or concentration $\bar{c}_d$ which is

assigned implicitly by controlling the external chemical potential μ_e. In (2.12) and (2.13), notation $\partial_s \mathcal{B}_d$ with $s = t$, u, q or c refers to the portion of the boundary of $\mathcal{B}_d$ where traction $\mathbf{t}$, displacement $\bar{\mathbf{u}}_d$, solvent source q_s, and concentration $\bar{c}_d$ are prescribed, respectively. Finally, Eqs. (2.14) are the initial conditions for the state variables $\mathbf{u}_d$ and c_d.

An easy solution of the stress-diffusion problem corresponds to a body which is embedded into a bath of assigned chemical potential μ_e and attains a swollen stress-free state. Then, $\mathbf{F}_d = \lambda_o \mathbf{I}$, $\mathbf{S}_d = \mathbf{0}$, and

$$\mathcal{R} T \left(\log \frac{\lambda_o^3 - 1}{\lambda_o^3} + \frac{1}{\lambda_o^3} + \frac{\chi}{\lambda_o^6} \right) + p\Omega = \mu_e, \qquad (2.15)$$

and λ_o identifies the uniform swelling ratio corresponding to a given shear modulus G_d once the external chemical potential μ_e and the Flory parameter χ have been fixed.

When $\lambda_o \gg 1$ (that is, $1/\lambda_o \ll 1$), Eq. (2.15) can be approximated, by estimating the leading order term in the asymptotic expansion up to $O\left(1/\lambda_o^8\right)$, as

$$\lambda_o = \left(\frac{\mathcal{R}T}{\Omega} \frac{1/2 - \chi}{G_d} \right)^{1/5}, \qquad (2.16)$$

corresponding to $\mu_e = 0$.

III. SWELLING AND DE-SWELLING CYCLES

We are interested in steady solutions of the problem (2.11)–(2.13), that is, such that $\mathrm{div} \, \mathbf{h}_d = 0$, corresponding to constraints and load free boundaries, that is, $\mathbf{t} = \mathbf{0}$ on $\partial \mathcal{B}_d \times \mathcal{T}$, and induced by swelling paths. The goal is to investigate the relationship between the curving of an initially flat and dry hydrogel structure and the change in the environmental conditions around it.

We start considering a thin hydrogel structure $\mathcal{B}_d$, represented as a beam in its stress-free and dry state embedded into a dry environment in the cartoon in Fig. 1 (top left). We change the chemical conditions of the environment by controlling the chemical potential on the bottom and top of the structure whereas assuming impermeable edges. So, the hydrogel may go from its flat dry to a flat fully wet state (Fig. 1, bottom right), when it is assumed as completely embedded in a homogeneously hydrated environment. Likewise, we can identify two curved steady states when the hydration conditions of the environment at the top and bottom of the beam are different (Fig. 1, top right and bottom left). In the last cases, the beam works as a pump draining water from the wet to the dry face of the beam.

The modeling of the swelling and de-swelling cycles is based on the theoretical background illustrated in Sec. II. Key elements of the computational implementation are the tackling of the chemical boundary conditions (2.13), which also involve the assignment of an external chemical potential μ_e. First, as it is not possible to control either the solvent source q_s at the surface or the surface concentration c_s, as is done in real experiments, we control the chemical potential μ_e of the bath. Equation (2.4), when evaluated at the boundary $\partial \mathcal{B}_c$, relates c_s to μ_e. It is a highly non-linear equation
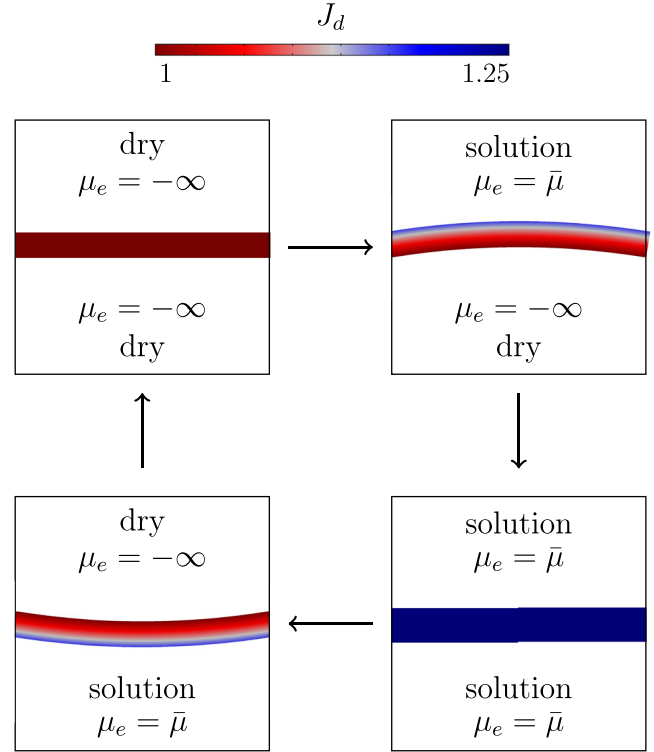

FIG. 1. Cycle of hydration and de-hydration of a gel: a homogeneous straight beam is embedded in a dry environment (top left panel); due to a change in the bath in contact with the top of the beam, it swells and attains a steady bent state (top left panel); a further change in the bath induces further swelling and a steady straight state is got (bottom right panel); a last change in the bath determines a swelling which brings the beam at a steady bent state with curvature opposite (bottom left panel). Colour code refers to J_d values. We assumed: $G_d = 10^8$ Pa and $\bar{\mu} = 0$.

which cannot be solved explicitly for c_s. On the other hand, the control of the state variable c_s, through Eq. (2.13)$_2$, forces the surface flux source q_s to be viewed as an unknown *a priori* reaction. The *a posteriori* evaluation of q_s yields poor approximations and suggested to us the following integral implementation of the boundary conditions (2.13):

$$0 = \int_{\partial_c \mathcal{B}_d} [\hat{\mu}(c_s) + p\,\Omega - \mu_e] \cdot \tilde{c}_s, \qquad (3.1)$$

$$0 = \int_{\partial_c \mathcal{B}_d} [(c_d - c_s)\tilde{q}_s + q_s(\tilde{c}_d - \tilde{c}_s)], \qquad (3.2)$$

which enforce the constraint $c_d = c_s$ by considering q_s as an additional state variable, having the role of a Lagrange multiplier, and provides a better numerical evaluation of the boundary source q_s.

In the following analysis, some of the physical quantities are fixed and get the values shown in Table I.

A. Beam-like pumps

We consider a beam-like body whose aspect ratio is $h/l = 0.1$, h being its thickness and width and l its length. The surface boundary $\partial \mathcal{B}$ is composed of a top $\partial \mathcal{B}_t$ surface and a bottom $\partial \mathcal{B}_b$ permeable surface and of the edges which are not permeable: $q_s = 0$. We start from a dry state which is also stress-free and induce a swelling process through a change in

TABLE I. Numerical values of the parameters.

Parameter	Symbol and value
Dis-affinity	$\chi = 0.4$
Molar volume	$\Omega = 1.8 \times 10^{-5}$ m^3/mol
Diffusivity	$D = 10^{-9}$ m^2/s
Temperature	$T = 293$ K
Length	$l = 1$ cm

the external conditions on the top surface. The corresponding steady state is a curved beam with constant curvature which works as a pump draining water from the top to the bottom surface. We assume to have infinite reservoirs in contact with the top and bottom surfaces; hence, we do not deal with any problems induced by the pump effect on a confined volume of water (see Ref. 13 for a detailed analysis of this kind of effect).

Anyway, the analysis of the steady curved state shows a few interesting characteristics. As first, the driving force of the process is the mismatch $\Delta\mu_e = \mu_e^t - \mu_e^b$ between the chemical potential's values at the top and bottom surfaces. We observe that increasing the mismatch makes the pattern of the chemical potential μ across the beam thickness steeper and steeper (Fig. 2). Moreover, due to the non-uniformity of the deformation field across the thickness and to the constitutive equations (2.9) and (2.10), the pattern of μ across the thickness of the beam is never linear, as it is sometimes assumed in literature.[22]

Second, the intensity of the pump, which can be measured by the amount of water crossing the top or the bottom surface per unit of time

$$\dot{V}_s = \int_{\partial \mathcal{B}_t} q_s \, dA_d, \quad [\dot{V}_s] = \text{m}^3/\text{s}, \qquad (3.3)$$

varies along the process. Figure 3 shows as along the transient the two quantities are not the same: the ingoing (solid red line) and outgoing (solid orange line) fluxes are always opposite in sign at the top and bottom surfaces, respectively and, at
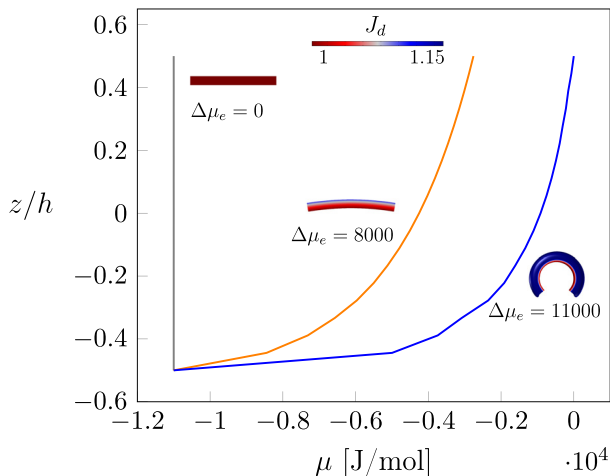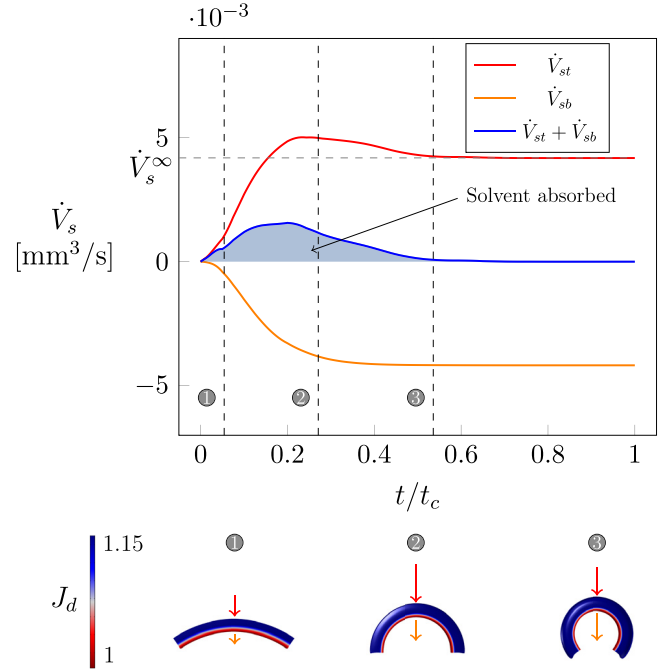
FIG. 3. Amount of water crossing the top ($\dot{V}_{st}$) and bottom ($\dot{V}_{sb}$) surface per unit of time (solid red and orange lines) and absorbed into the beam (grey area) along the process. After a time $t < 0.6\,t_c$ the process is steady: the ingoing and outgoing fluxes are equal. We assumed: $G_d = 10^5$ Pa.

any time t, the difference between the two quantities delivers the amount of water absorbed by the beam (grey area). At the steady state, the two fluxes are equal and the amount of absorbed water is zero; hence, the beam works just as an osmotic pump draining water from the top to the bottom. In representing the transient process (Fig. 3), a characteristic time t_c has been introduced as $t_c = ((l + 2h)/3)^2/D$ to evidence the duration of the transient part of the process with respect to the full time interval $t = t_c$.

Finally, the steady configuration attained by the beam is characterized by a constant curvature which can be measured in terms of the mismatch $\Delta\mu_e$. Figure 4 shows as higher is the mismatch, higher is the beam curvature (red and blue circles). Moreover, it also shows that softer beam (red circles) realizes higher curvature than stiffer beam (blue circles). Red and blue solid lines in Fig. 4 represent the beam curvature corresponding to the same shear moduli corresponding to red and blue circles, as delivered by the explicit analysis presented in Sec. IV.
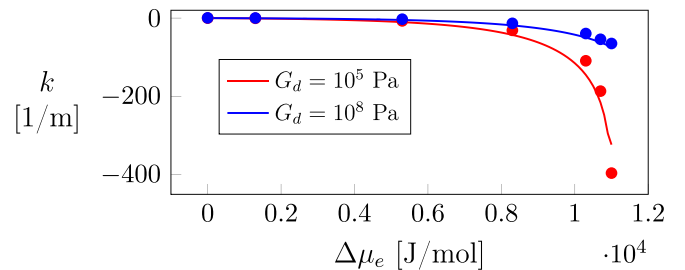
FIG. 2. Pattern of the chemical potential μ across the thickness of the beam for different values of $\Delta\mu_e$: higher $\Delta\mu_e$ steeper the pattern and more bent the beam (see the insets). Colour code refers to values of J_d. We assumed: $G_d = 10^5$ Pa.

FIG. 4. Beam curvature κ versus the mismatch $\Delta\mu_e$ is represented as a red and blue circle, depending on the value of the shear modulus. Red and blue solid lines represent the beam curvature corresponding to the same shear moduli as delivered by the explicit analysis presented in Sec. IV.

B. Plate-like pumps

We consider a plate-like body whose aspect ratio is $h/l = 0.1$, l being the length of plate's sides, having the edges which are not permeable and the top $\partial \mathcal{B}_t$ and bottom $\partial \mathcal{B}_b$ faces which are permeable surfaces. We start from a dry state which is also stress-free and induces a process like the one described for the beam-like body. At the steady state, the flat sheet is dome-shaped, characterized by an almost constant Gaussian curvature K, and drains water from the top to the bottom surface. The Gaussian curvature of the curved surface is represented in Fig. 5 (top panel) in terms of the mismatch $\Delta \mu_e$ through the mean value $\bar{K}$ on the middle surface of the plate (blue circles) and the value $K^\star$ at the middle point of the middle plane (red diamonds). The two values are very close up to certain values of $\Delta \mu_e$; then, they start going far one from each other and the difference between $\bar{K}$ and $K^\star$ increases with $\Delta \mu_e$. Indeed, for large $\Delta \mu_e$ we have a large stretching of the middle plane and the Gaussian curvature takes extremely high values on the boundary of the dome-like shape, which also loses its spherical symmetry, as Fig. 5 (bottom panel) shows through a colour code corresponding to the local value of K. The solid line in Fig. 5 (top panel) corresponds to the explicit solution presented in Sec. IV.

At the steady state, the plate realizes shows a gradient of chemical potential μ across the thickness going from the bottom value (μ_e^b, red) to the top value (μ_e^t, blue) [Fig. 5 (middle panel)].

IV. STEADY BENDING IN HOMOGENEOUS HYDROGEL BEAMS AND PLATES

We propose an approximate analysis of the steady solutions of the stress–diffusion problem of the homogeneous hydrogel beam borrowed from the study proposed for bilayered beams embedded in a homogeneous bath in Ref. 2 (see also Refs. 3, 4, and 23). Therein, bending was induced by embedding into a bath of assigned chemical potential $\mu_e = 0$ a bilayer beam made by two layers of different materials: the ratio $\beta = h_t/h$ between the thickness of the top layer and the beam thickness and the ratio $\alpha = G_t/G_b$ between the shear moduli of the two layers played a key role in the analysis. Only the longitudinal deformation λ of the beam was taken into account in the description of the bent state. It was multiplicatively decomposed in a uniform free-swelling ratio that would take place if the part were free from the rest of the beam and a further elastic component. In particular, the uniform free-swelling components of each part were determined from the appropriate mechano–chemical equilibrium equations as if the beam was made of two independent layers free to swell as much as they like, according to the shear modulus. On its side, the elastic deformations resulted from the multiplicative decomposition once the global compatibility of the bending deformation has been ensured. These latter determined internal stresses corresponding, in the absence of external forces, to null forces and torques on each cross section of the beam. The analysis delivered a Timoshenko-like formula for the swelling-induced curvature κ of the beam axis, as well as a formula for the swelling-induced stretch Λ_o of the beam axis.
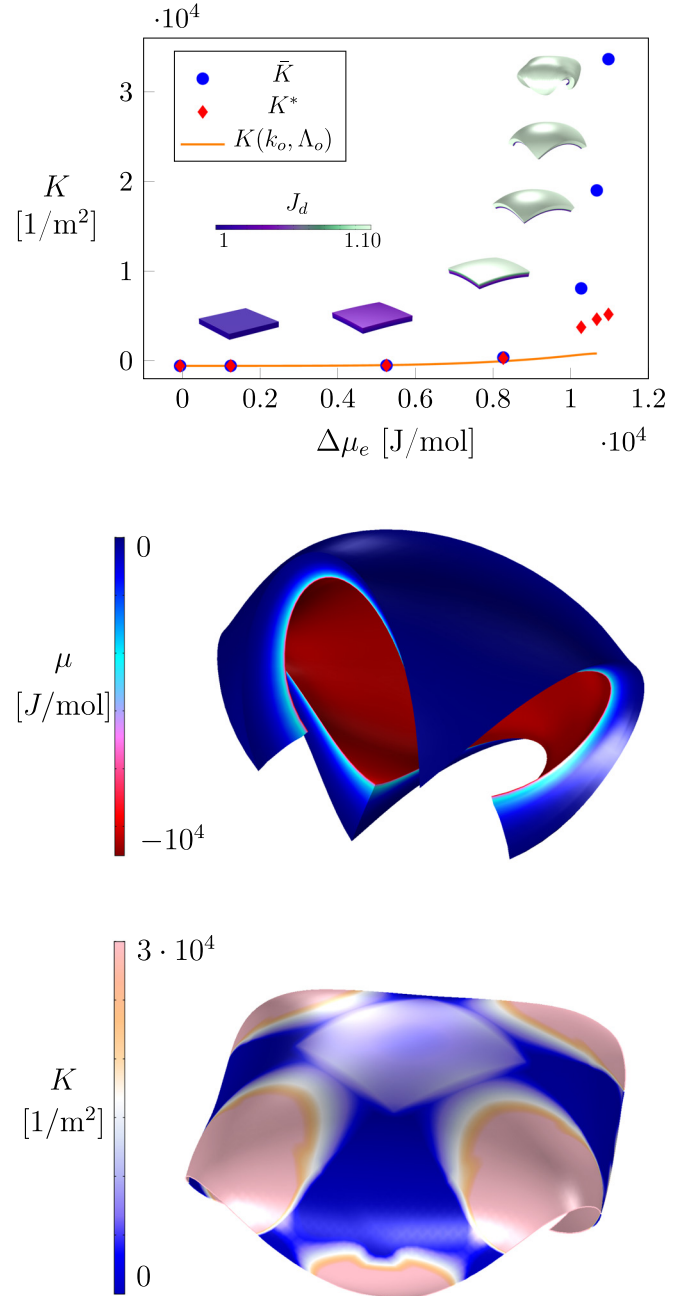

FIG. 5. Gaussian curvature K versus the mismatch $\Delta \mu_e$ is represented through the mean value $\bar{K}$ of K on the middle surface of the plate (blue circles), the value $K^\star$ at the middle point of the middle plane (red diamonds); the red solid line represents the Gaussian curvature as delivered by the explicit analysis presented in Sec. IV (top panel). Steady curved shape of a square plate: colour code refers to chemical potential (middle panel) and to Gaussian curvature (bottom panel). We assumed: $G_d = 10^5$ Pa.

In the present problem, we have a homogeneous beam whose steady state is curved and characterized by a hydration level which is not uniform across the thickness. As it is expected, the chemical potential is not homogeneous neither linear along the thickness (see Fig. 2), going from the value μ_e^b at the bottom to the value μ_e^t at the top. As described by the cartoon in Fig. 6, we identify two layers of thickness $h_t = \beta h$ (top layer) and $h_b = (1 - \beta)h$ (bottom layer) where the chemical potential is constant and equal to the top and bottom values, respectively, by introducing the piecewise constant function
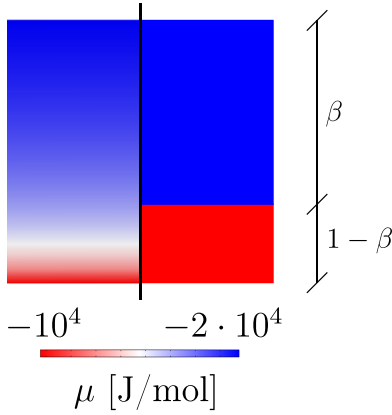
FIG. 6. Chemical potential μ changes across the thickness from the bottom value μ_e^b (red) to the top value μ_e^t (blue) (left side of the cartoon). This distribution is replaced by one that is piecewise constant (right side of the cartoon).

$$\mu_{cst}(x_3) = \begin{cases} \mu_e^t & \text{for } h/2 - \beta h < x_3 < h/2, \\ \mu_e^b & \text{for } -h/2 < x_3 < h/2 - \beta h, \end{cases}$$

$x_3 = 0$ being the geometrical beam axis. The value of the parameter β which determines the two layers's thicknesses comes from the following identity:

$$\int_{\mathcal{B}_d} \frac{\mu}{\Omega} dV = \frac{\mu_e^t}{\Omega} V_t + \frac{\mu_e^b}{\Omega} V_b, \tag{4.1}$$

$V_t = \beta hLw$ and $V_b = (1 - \beta)hLw$ being the volumes of the top and bottom layer, respectively, and μ the not homogeneous chemical field across the beam. Identity (4.1) says that the amount of work required to move all the volume of solvent from the top to the bottom face in the actual beam [left hand-side of identity (4.1)] is equal to the work done in the beam once assumed the chemical potential separately homogeneous in the two layers identified by the parameter β [right hand-side of identity (4.1)].[24] It can be written as

$$\int_{-h/2}^{h/2} \mu(x_3)dx_3 = \mu_e^t \beta h + \mu_e^b (1 - \beta) h. \tag{4.2}$$

To determine the parameter β from the identity (4.2), we need the explicit representation of the chemical potential field μ across the beam, and we get an approximate expression for μ into few steps. First, inspired by the numerical results, we explicitly represent $\mu(x_3)$ by a quadratic function of x_3 as

$$\mu(x_3) = \mu_0 + x_3\mu_1 + x_3^2\mu_2, \tag{4.3}$$

in terms of the three scalars μ_0, μ_1, and μ_2. Second, we determine the three scalars by requiring that the following key boundary conditions are satisfied. The first two conditions are

$$\mu(h/2) = \mu_e^t \quad \text{and} \quad \mu(-h/2) = \mu_e^b. \tag{4.4}$$

The third condition comes from the solvent flux $\mathbf{h}_d = q\mathbf{e}_3$ which is constant across the beam at the steady state, hence, such that

$$q(h/2) = q(-h/2). \tag{4.5}$$

On the other hand, from Eqs. (2.9) and (2.10), we get

$$q(x_3) = -\frac{D}{RT} \frac{c_d(x_3)}{\lambda_3^2(x_3)} \mu'(x_3), \tag{4.6}$$

and with this, Eq. (4.5) can be written as

$$\left(\frac{c_d}{\lambda_3^2} \mu' \right)_{h/2} = \left(\frac{c_d}{\lambda_3^2} \mu' \right)_{-h/2}. \tag{4.7}$$

Finally, we assume that $\lambda_3(h/2) = \lambda_{ot}$ and $\lambda_3(-h/2) = \lambda_{ob}$, with $\lambda_{ot} = \lambda_{ot}(G_d, \mu_e^t)$ and $\lambda_{ob} = \lambda_{ob}(G_d, \mu_e^b)$ the swelling ratios which satisfy the equations

$$\frac{G_d\Omega}{\lambda_{oi}} + RT \left(\log \left(1 - \frac{1}{(\lambda_{oi})^3} \right) + \frac{1}{(\lambda_{oi})^3} + \frac{\chi}{(\lambda_{oi})^6} \right) = \mu_e^i, \tag{4.8}$$

with $i = t, b$; and that $1 + \Omega c_d(h/2) = (\lambda_{ot})^3$, and $1 + \Omega c_d(-h/2) = (\lambda_{ob})^3$. With this, Eq. (4.7) can be written as

$$\mu'(h/2) = C_o \mu'(-h/2), \tag{4.9}$$

with[25]

$$C_o = \frac{(\lambda_{ot})^2((\lambda_{ob})^3 - 1)}{(\lambda_{ob})^2((\lambda_{ot})^3 - 1)}, \tag{4.10}$$

and it prescribes that the third condition which added to the first two conditions given by Eq. (4.4) allows determining the unknown coefficients μ_i with $i = 0, 1, 2$. With this, Eq. (4.1) allows to determine β as

$$\beta = \frac{2 + C_o}{3(1 + C_o)}. \tag{4.11}$$

From now on, we view the homogeneous beam as a bilayer beam whose layers of thickness $h_t = \beta h$ and h_b are swollen up to a level determined by the chemical potential μ_e at the top and bottom face, as Eq. (2.15) prescribes: precisely, we have $\mu = \mu_e^t$ and $\mu = \mu_e^b$ in the top and bottom layer, respectively (see Fig. 6). As in Ref. 2, we assume that the longitudinal deformation $\lambda(x_3) = \Lambda_0(1 - x_3\Lambda_0\kappa)$ of the beam can be viewed as the product of the free-swelling ratio due to the hydration level and an elastic component which deliver internal stresses. So, given the free-swelling ratios λ_{ot} and λ_{ob} above introduced, the corresponding elastic deformations $\lambda_{et} = \lambda\lambda_{ot}^{-1}$ and $\lambda_{eb} = \lambda\lambda_{ob}^{-1}$ are determined from the multiplicative decomposition in terms of Λ_o and κ.

Then, assuming zero out-of-plane stresses, the corresponding longitudinal stresses σ_t and σ_b on the cross-sections of the top and bottom layers, respectively, are evaluated as

$$\sigma_t(x_1, x_3) = 3G_d(\lambda(x_1, x_3)\lambda_{ot}^{-1} - 1), \tag{4.12}$$

for $(h/2 - \beta h) < x_3 < h/2$; and

$$\sigma_b(x_1, x_3) = 3G_d(\lambda(x_1, x_3)\lambda_{ob}^{-1} - 1), \tag{4.13}$$

for $-h/2 < x_3 < (h/2 - \beta h)$, where, due to the material incompressibility, $3G_d$ identifies the corresponding Young modulus.

We looked for free-swelling solutions of the gel beam problem: under no external loads, the resultant $F(\lambda_{ob}, \lambda_{ot})$ of the stresses and the resultant moment $M(\lambda_{ob}, \lambda_{ot})$ of the stresses on the gel beam have to be identically null, that is,

$$F(\lambda_{ob}, \lambda_{ot}) = 0 \quad \text{and} \quad M(\lambda_{ob}, \lambda_{ot}) = 0. \qquad (4.14)$$

Equation (4.12) delivers a linear system of two equations in Λ_0 and $\Lambda_1 = \kappa \Lambda_0^2$ where, differently from the situation studied in Ref. 2, the parameter β is not geometrically but thermodynamically determined. Moreover, the two layers of the beam being made of the same material, the ratio α between the shear moduli of the two layers is 1 and the bending is driven by the mismatch $\Delta \mu_e$. The solution delivers the beam stretching Λ_0 and curvature κ as the following functions:

$$\Lambda_0 = \Lambda_0(\lambda_{ot}, \lambda_{ob}, \beta) \quad \text{and} \quad \kappa = \kappa(\lambda_{ot}, \lambda_{ob}, \beta), \qquad (4.15)$$

explicitly represented in the Appendix. Given the relations

$$\mathcal{R} T \left(\log \frac{\lambda_{om}^3 - 1}{\lambda_{om}^3} + \frac{1}{\lambda_{om}^3} + \frac{\chi}{\lambda_{om}^6} \right) + \frac{G_d \Omega}{\lambda_{om}} = \mu_e^m \qquad (4.16)$$

$(m = b, t)$ between the free-swelling stretches λ_{ot} and λ_{ob} and the top and bottom chemical potential μ_e^t and μ_e^b, and fixed μ_e^b, Eq. (4.15) delivers $\Lambda_0(G_d, \Delta \mu_e)$ and $\kappa(G_d, \Delta \mu_e)$. Fixed the value $\mu_e^b = -11\,000$ J/mol, the beam curvature is so evaluated starting from the value $\Delta \mu_e = 0$ corresponding to $\mu_e^t = -11\,000$ J/mol. It is represented by the solid lines in Fig. 4 for $G_d = 10^5$ Pa (red) and $G_d = 10^8$ Pa (blue); it can be appreciated the good agreement between the explicit and the numerical solution which is excellent for values of $\Delta \mu_e$ not too much high.

A. Cutting a beam out of the plate

As the last step, we propose an explicit formula delivering the Gaussian curvature of the plate-like pump at the steady state. In this case, the body is modeled within the setting of non-Euclidean plates as a shell with its first and second natural fundamental forms. The first and second fundamental forms **a** and **b** contain all the information about lateral distances between points and local curvature, respectively; the natural forms $\bar{\mathbf{a}}$ and $\bar{\mathbf{b}}$ represent the lateral distances and curvatures that would make the sheet locally stress-free, and they are determined by the specific stimulus which in this case is the mismatch $\Delta \mu_e$. Due to the differential isotropic expansion of the two layers due to the swelling, the lateral distances would like to stretch by a_o while the midplane would like to bend with a curvature b_o in every direction, and $\bar{\mathbf{a}}$ and $\bar{\mathbf{b}}$ have the following form:

$$\bar{\mathbf{a}} = a_o^2 \begin{pmatrix} 1 & 0 \\ 0 & 1 \end{pmatrix} \quad \text{and} \quad \bar{\mathbf{b}} = b_o \begin{pmatrix} 1 & 0 \\ 0 & 1 \end{pmatrix}. \qquad (4.17)$$

It is not usually possible for a sheet to realize both natural forms, due to the Gauss-Codazzi-Mainardi equations, and this is the case of our plate which has to match different planes across the thickness which would like to swell according to a different value of the chemical potential. However, as a beam is able to adopt its natural shape with longitudinal axis stretch and curvature equal to Λ_0 and κ, respectively, without any need of satisfying additional constraints, we proceed by cutting a beam from the plate disk and by measuring its deformed shape. This will provide a straightforward way to evaluate the natural stretch and curvature of the disk[8,9]

$$a_o = \Lambda_0(G_d, \mu_e^b, \Delta \mu_e), \quad b_o = \kappa(G_d, \mu_e^b, \Delta \mu_e). \qquad (4.18)$$

Assuming as usual for non-Euclidean plates, a Kirchhoff-Love energy density, the energy of the plate can be written as

$$\bar{\mathcal{U}} = \int (\text{tr}(\mathbf{a} - \bar{\mathbf{a}})^2 + \text{tr}^2(\mathbf{a} - \bar{\mathbf{a}})) \sqrt{\bar{\mathbf{a}}} \, dA$$
$$+ \int (\text{tr}(\mathbf{b} - \bar{\mathbf{b}})^2 + \text{tr}^2(\mathbf{b} - \bar{\mathbf{b}})) \sqrt{\bar{\mathbf{a}}} \, dA,$$

being $\bar{\mathcal{U}} = 8\mathcal{U}(1 - \nu^2)/Eh$, E and μ the Young and Poisson moduli, and **a** and **b** the first and second fundamental forms of the midsurface of the deformed plate, respectively. We follow Ref. 9 and assume a metric with constant Gaussian curvature in Gaussian normal coordinates (see also Ref. 26); we also assume that $\nu \simeq 1/2$ and $E \simeq 3G$. So, the total dimensionless energy for the square disk of side l is

$$\bar{\mathcal{U}} = \frac{1}{9} L^4 \Lambda_0^{-2} \int r^4 dA + h^2 A \Lambda_0^{-2} (L - \kappa)^2, \qquad (4.19)$$

being Λ_0 and κ given by Eq. (4.15), and L the principal curvature of the sphere. Following Ref. 9, we also assumed that the Gaussian curvature can be approximated as

$$K = \det \mathbf{b} / \det \mathbf{a} \simeq \frac{L^2}{\Lambda_o^4}. \qquad (4.20)$$

Minimization of the total energy $\bar{\mathcal{U}}$ with respect to L yields

$$\bar{L}^3 + \gamma^4 (\bar{L} - \bar{\kappa}) = 0, \qquad (4.21)$$

being $\bar{L} = Lh$, $\bar{\kappa} = \kappa h$, and

$$\gamma^4 = \frac{h^4}{\mathcal{S}^4}, \quad \mathcal{S}^4 = \frac{2}{9} \frac{1}{A} \int r^4 dA. \qquad (4.22)$$

Moreover, it holds

$$A = l^2, \quad \mathcal{S}^4 = \frac{56}{405} l^4, \quad \gamma^4 = \frac{405}{56} \frac{h^4}{l^4}. \qquad (4.23)$$

Equation (4.21) can be solved explicitly and delivers $\bar{L} = \bar{L}(\kappa)$. From there, using Eq. (4.20), we get

$$K = K(\Lambda_0, \kappa), \qquad (4.24)$$

which can be ultimately expressed in terms of the mismatch $\Delta \mu_e$ using Eqs. (4.15) and (4.16). In Fig. 5, we represented the function $K(\Delta \mu_e)$, corresponding to a fixed value of

$G_d = 10^8$ Pa. The agreement with the mean values of K as well as with the Gaussian curvature at the middle of the plate is good if the mismatch $\Delta\mu_e$ does not grow too much. Indeed, for large $\Delta\mu_e$ we have: (1) $\bar{K}$ and $K^\star$ differs a lot due to the large values attained by the Gaussian curvature on the corner of the plate; (2) the stretching of the midsurface increases and the approximation (4.20) does not hold any more.

V. CONCLUSIONS

In the last few years, swelling-induced morphing of flat thin sheets has attracted more and more attention of the scientific community which has elaborated accurate numerical tools to implement a stress diffusion model which is thermodynamically consistent with the Flory-Rehner thermodynamics and able to describe the huge deformation occurring in swelling processes (see Refs. 10–13 and 27). Moreover, in some distinguished cases, also explicit formulas have been proposed able to catch the morphing behaviour of swelling thin sheets under some limitations (see Refs. 2–4 and 23).

However, typically almost all of the analyses refer to a situation which is completely homogeneous on the boundary of the body and the driving force which realizes that the morphing of flat sheets in curved configuration is the swelling mismatch in different parts of the body. Prototypical problems are concerning bending in layered beams and plates.

Here, we studied a different kind of problem where morphing of homogeneous beams and plates is driven by different environment conditions: a mismatch in the chemical potential on the opposite faces of the structure drives a swelling and determines curved steady states. We proposed both theoretical and computational approaches to describe the behaviour of these hydrogel devices, getting interesting insights into their performances.

ACKNOWLEDGMENTS

APPENDIX: BEAM'S STRETCHING AND CURVATURE

Equation (4.14) delivers the beam stretching Λ_0 and curvature κ as

$$\Lambda_0 = \Lambda_0(\lambda_{ot}, \lambda_{ob}, \beta) \quad \text{and} \quad \kappa = \kappa(\lambda_{ot}, \lambda_{ob}, \beta), \quad (A1)$$

with

$$\Lambda_0(\lambda_{ot}, \lambda_{ob}, \beta) = (\beta^4\lambda_{ot}^3 + (\beta - 1)^4\lambda_{ob}^3$$
$$+ \beta(1 - \beta)a(\beta)\lambda_{ob}^2\lambda_{ot}$$
$$+ \beta(1 - \beta^3)\lambda_{ob}\lambda_{ot}^2)D(\lambda_{ot}, \lambda_{ob}, \beta)^{-1}, \quad (A2)$$

$$\Lambda_1(\lambda_{ot}, \lambda_{ob}, \beta) = -6\beta(\beta - 1)\lambda_{ob}\lambda_{ot}$$
$$\times (\lambda_{ob} - \lambda_{ot})(hD(\lambda_{ot}, \lambda_{ob}, \beta))^{-1}, \quad (A3)$$

$$\kappa(\lambda_{ot}, \lambda_{ob}, \beta) = \frac{\Lambda_1(\lambda_{ot}, \lambda_{ob}, \beta)}{\Lambda_0(\lambda_{ot}, \lambda_{ob}, \beta)^2}, \quad (A4)$$

and

$$D(\lambda_{ot}, \lambda_{ob}, \beta) = \beta^4\lambda_{ot}^2 + (\beta - 1)^4\lambda_{ob}^2$$
$$+ \beta(1 - \beta)d(\beta)\lambda_{ob}\lambda_{ot}, \quad (A5)$$

where we set $a(\beta) = 3 + \beta(\beta - 3)$ and $d(\beta) = 2\beta^2 - 2\beta + 4$. The free-swelling stretches λ_{ot} and λ_{ob} come from the chemical equilibrium equation (4.8) in terms of the shear modulus of the beam and the top and bottom chemical potential μ_e^t and μ_e^b.

[1]T. van Manen, S. Janbaz, and A. A. Zadpoor, "Programming the shape-shifting of flat soft matter," Mater. Today **21**, 144–163 (2018).

[2]A. Lucantonio, P. Nardinocchi, and M. Pezzulla, "Swelling-induced and controlled curving in layered gel beams," Proc. R. Soc. A: Math., Phys. Eng. Sci. **470**, 20140467 (2014).

[3]P. Nardinocchi and E. Puntel, "Unexpected hardening effects in bilayered gel beams," Meccanica **52**, 3471–3480 (2017).

[4]P. Nardinocchi and E. Puntel, "Swelling-induced wrinkling in layered gel beams," Proc. R. Soc. London A: Math., Phys. Eng. Sci. **473**, 20170454 (2017).

[5]P. Nardinocchi, M. Pezzulla, and L. Teresi, "Anisotropic swelling of thin gel sheets," Soft Matter **11**, 1492–1499 (2015).

[6]D. P. Holmes, M. Roche, T. Sinha, and H. A. Stone, "Bending and twisting of soft materials by non-homogenous swelling," Soft Matter **7**, 5188–5193 (2011).

[7]A. Pandey and D. P. Holmes, "Swelling-induced deformations: A materials-defined transition from macroscale to microscale deformations," Soft Matter **9**, 5524–5528 (2013).

[8]S. Armon, E. Efrati, R. Kupferman, and E. Sharon, "Geometry and mechanics in the opening of chiral seed pods," Science **333**, 1726–1730 (2011).

[9]M. Pezzulla, G. P. Smith, P. Nardinocchi, and D. P. Holmes, "Geometry and mechanics of thin growing bilayers," Soft Matter **12**, 4435–4442 (2016).

[10]A. Lucantonio, P. Nardinocchi, and L. Teresi, "Transient analysis of swelling-induced large deformations in polymer gels," J. Mech. Phys. Solids **61**, 205–218 (2013).

[11]A. Lucantonio, M. Roche, P. Nardinocchi, and H. A. Stone, "Buckling dynamics of a solvent-stimulated stretched elastomeric sheet," Soft Matter **10**, 2800–2804 (2014).

[12]M. Curatolo, P. Nardinocchi, E. Puntel, and L. Teresi, "Transient instabilities in the swelling dynamics of a hydrogel sphere," J. Appl. Phys. **122**, 145109 (2017).

[13]M. Curatolo, P. Nardinocchi, and L. Teresi, "Driving water cavitation in a hydrogel cavity," Soft Matter **14**, 2310–2321 (2018).

[14]W. Hong, X. Zhao, J. Zhou, and Z. Suo, "A theory of coupled diffusion and large deformation in polymeric gels," J. Mech. Phys. Solids **56**, 1779–1793 (2008).

[15]W. Hong, Z. Liu, and Z. Suo, "Inhomogeneous swelling of a gel in equilibrium with a solvent and mechanical load," Int. J. Solids Struct. **46**, 3282–3289 (2009).

[16]J. Zhang, X. Zhao, Z. Suo, and H. Jiang, "A finite element method for transient analysis of concurrent large deformation and mass transport in gels," J. Appl. Phys. **105**, 093522 (2009).

[17]S. A. Chester and L. Anand, "A coupled theory of fluid permeation and large deformations for elastomeric materials," J. Mech. Phys. Solids **58**, 1879–1906 (2010).

[18]We use the notation, [α] to indicate the SI units of a quantity α.

[19]P. J. Flory and J. Rehner, "Statistical mechanics of cross-linked polymer networks i. rubberlike elasticity," J. Chem. Phys. **11**, 512–520 (1943).

[20]P. J. Flory and J. Rehner, "Statistical mechanics of cross-linked polymer networks ii. swelling," J. Chem. Phys. **11**, 521–526 (1943).

[21]It is worth noting that $q_s > 0$ corresponds to a positive source, that is, an inward flux.

[22]A. Lucantonio, G. Tomassetti, and A. DeSimone, "Large-strain poroelastic plate theory for polymer gels with applications to swelling-induced morphing of composite plates," Composites Part B **115**, 330–340 (2017). Composite lattices and multiscale innovative materials and structures.

[23]P. Nardinocchi and E. Puntel, "Finite bending solutions for layered gel beams," Int. J. Solids Struct. **90**, 228–235 (2016).

[24]It is identified with the corresponding volume of the beam occupied by the solvent.

[25]It is worth noting that Co depends on μ_e^t and μ_e^b through Eq. (4.8).

[26]M. Pezzulla, S. A. Shillig, P. Nardinocchi, and D. P. Holmes, "Morphing of geometric composites via residual swelling," Soft Matter **11**, 5812–5820 (2015).

[27]A. Lucantonio, P. Nardinocchi, and H. A. Stone, "Swelling dynamics of a thin elastomeric sheet under uniaxial pre-stretch," J. Appl. Phys. **115**, 083505 (2014).